

Article

Augmented Reality on the Large Scene Based on a Markerless Registration Framework

Zhen Ma, He Xu *, Yonghui Zhang, Junlong Chen, Dongbo Zhao, Siqing Chen

College of Mechanical and Electrical Engineering, Harbin Engineering University, Harbin 150001, China;

* Correspondence: railway_dragon@163.com; Tel.: +86-1-335-111-7608

Abstract: In this paper, a mobile camera positioning method based on forward and inverse kinematics of robot is proposed, which can realize far point positioning of imaging position and attitude tracking in large scene enhancement. Orbit precision motion through the framework overhead cameras and combining with the ground system of sensor array object such as mobile robot platform of various sensors, realize the good 3 d image registration, solve any artifacts that is mobile robot in the large space position initialization problem, effectively implement the large space no marks augmented reality, human-computer interaction, and information summary. Finally, the feasibility and effectiveness of the method are verified by experiments.

Keywords: large-scale scene; augmented reality; markerless; kinematics

1. Introduction

Augmented reality provides new tools for human-based control and interaction with complex systems. Users' sensory physical experience is combined with information from digital systems to achieve a good experience for users [1-4].

In the process of industrial production, especially the assembly of large mechanical equipment such as aircraft, such problems can be effectively solved through the augmented reality of large scenes [5-7]. In the augmented reality display of large scenes, the marked method is very sensitive to factors such as disturbing light and visibility, and the use of marking will cause interference to the scene environment and directly affect the user experience [8-13]. For example, under the condition of 220 lx-ray intensity, the maximum recognition distance of 80×80mm custom square sign is 1.70m. The rectangular QR mark with a size of 80×400mm has a maximum recognition distance of only 1.58m under 220lx-ray intensity, which is not conducive to augmented reality observation in complex environments [14-17]. In the case of large scene blocks, only the stable tracking of the camera can accurately determine the superposition position of the augmented reality and obtain a good user visual experience [23-25].

Problems and challenges are aimed, under the condition of large scene, put forward a identification method of augmented reality, use positioning mobile camera and the ground track has placed on encoder sensor system, adopts the frame camera position of kinematics transform method, get big artifacts in the scene (this article is based on water hydraulic flexible manipulator and the mobile robot as an example) long-distance increase origin detailed scene

of tracking and positioning, and in a large and touch screen to achieve the real-time information feedback of artifacts in the scene augmented reality and interaction. The method is suitable for industrial environments with poor optical environment and many interference conditions.

The paper is organized as follows. In section 2, The work of untagged augmented reality will be covered. In the third part, it describes the whole system, introduces the theoretical model of coordinate transformation, the mathematical formula of virtual image position conversion and the generation of the screen image. In section 4, the hardware (mechanical, control) and software components of the system are described. The fifth part carries on the theoretical verification through two experiments. The conclusions and future work are contained in section 6.

2. Related Work

SLAM is a typically untagged approach that tracks camera movements in real-time and builds virtual images in unprepared environments. Klein et al. [30] proposed a lens and real-time tracking system, which is a breakthrough method. However, it has a large cumulative error and is only suitable for scene tracking with small drift accumulation. Also, all these vision-based SLAM methods are still prone to system crashes due to moving blurred or text-based images [31-33].

To overcome the above single-lens vision obstacle [26], Wei fang et al. developed a real-time six-degree-of-freedom tracking method. A wide angle monocular camera and an inertial sensor are combined to achieve better robust six-degree-of-freedom motion tracking through mutual compensation between heterogeneous sensors. However, the method has a large cumulative drift error and weak anti-interference ability [34] [35].

3. Framework of Augmented Reality with Markerless Registration Based on Robotic Kinematics

Based on the inverse kinematics theory, the position points corresponding to the motion camera are obtained by understanding the end position and attitude of the augmented reality observation. High precision displacement sensor is used instead of the traditional visual recognition method, which is independent of good light, has strong anti-interference ability and small cumulative error, and can be widely used in various large scenes such as the industrial environment.

This paper presents a large scene augmented reality method based on laser encoder track. Different from the traditional SLAM[36] [37], this scheme only requires the use of an encoder and a ground displacement sensor. It can effectively solve the drift of the camera motion position and the accumulated error of the system. And Can be widely used in a variety of large - scale scenarios such as industrial manufacturing environment.

3.1. Kinematic Scene Coordinate Transformation Model

Large space coordinate measuring system based on unmarked modeling, to let the augmented reality of virtual as appeared on the appropriate display position, we design a calculation method based on the kinematics coordinate system conversion, set up the workpiece coordinate system and the corresponding characteristic as point on the camera image plane mapping between the model, so as long as the gain and camera artifacts stance,

after coordinate transformation is used in the overall system of coordinates of measuring points and import the unity 3 d.

3.1.1 The Components of the System's Coordinate System

It is necessary to establish five coordinate systems: the global coordinate system, the workpiece coordinate system, the camera coordinate, and the screen coordinate system. As shown in figure 1.

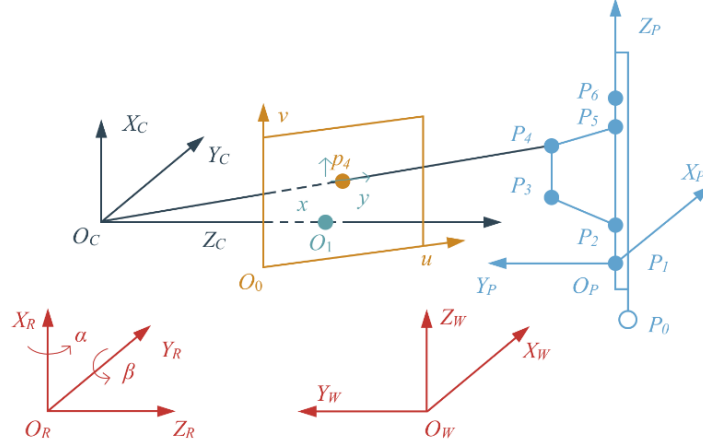


Figure 1. The model of coordinate system

1) The global coordinate system $C_w(O_w, X_w, Y_w, Z_w)$ based on the orbital frame: as the reference frame in the whole application environment, it is used to describe the position and attitude of the camera, the position and attitude of the workpiece and the display position of the screen. Points in the global coordinate system are represented as $P_w = (X_w, Y_w, Z_w)^T$.

2) The workpiece coordinate system $C_p(O_p, X_p, Y_p, Z_p)$ based on the placement direction of the workpiece: the origin O_p of the coordinate system is established on the first feature point of the workpiece, and the connection direction of the 1st and 5th points is taken as the positive direction of axis Z ; The axis Y is defined by the plane formed by points 1, 3 and 5, and the direction of axis X is determined by the right-hand rule. The spatial points in the workpiece coordinate system are represented as $P_p = (X_p, Y_p, Z_p)^T$.

3) Camera coordinate system $C_c(O_c, X_c, Y_c, Z_c)$ the origin of the coordinate system O_c is established at the perspective projection center of the camera. The axes X and Y correspond to the X_c -axis and Y_c -axis parallel to the image plane coordinate system. The point in camera coordinates is represented as $P_c = (X_c, Y_c, Z_c)^T$.

4) Screen coordinate system: the screen coordinate system is divided into two types. (u, v) represents the image coordinate system $C_o(O_o, uv)$ with pixels as the unit. The origin O_o is located at the upper left corner of the image plane. (x, y) represents the image coordinate system $C_1(O_1, xy)$ in millimeters, whose origin O_1 is located at the intersection of the camera optical axis and the image plane. The X -axis and Y -axis are parallel to the horizontal and vertical axes of the pixel respectively. O_1 in C_o coordinates is (u_0, v_0) .

5) Camera cradle frame coordinate system $C_r(O_r, X_r, Y_r, Z_r)$: the coordinate system origin O_r is established at the intersection of the two rotating axes of the turntable, and the rotation angles of Z_r and Y_r of the two rotating axes at a certain time are used to determine the attitude of the turntable coordinate system C_r in the reference system C_w . There is a rigid connection between the camera and the cradle head.

The camera coordinate system and the cradle head coordinate system are fixed and constant, generally only the translation relationship. The spatial points in the coordinate system of the turntable are represented as $P_r = (X_r, Y_r, Z_r)^T$

3.1.2 Transformation of Coordinate Points

Assuming that the coordinates of the space point in the two coordinate systems are respectively $P_1 = (X_1, Y_1, Z_1)^T$ and $P_2 = (X_2, Y_2, Z_2)^T$, then the following formula for the pose transformation can be obtained:

$$P_1 = RP_2 + T \quad (1)$$

where

$$R = \begin{bmatrix} r_{11} & r_{12} & r_{13} \\ r_{21} & r_{22} & r_{23} \\ r_{31} & r_{32} & r_{33} \end{bmatrix} \quad (2)$$

where

$$T = (t_x, t_y, t_z)^T \quad (3)$$

The point is represented by the homogeneous coordinate $P = (X, Y, Z, 1)^T$, and the pose transformation formula is converted into the following form:

$$P_1 = \begin{bmatrix} R & T \\ 0 & 1 \end{bmatrix} P_2 = M_{21} P_2 \quad (4)$$

where M_{12} is the pose matrix from frame 2 to frame 1.

Euler angles are represented by only three independent angles (roll, position, and angle), as shown in figure 2.

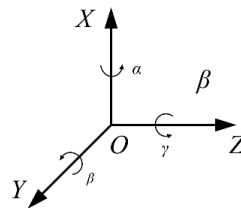


Figure 2. Euler angle parameterization

Under certain conditions, any attitude of the coordinate system can be uniquely represented by a set of Euler angles:

$$R_{xy} = \begin{bmatrix} \cos \beta \cos \gamma & \sin \alpha \sin \beta \cos \gamma - \cos \alpha \sin \gamma & \cos \alpha \sin \beta \cos \gamma + \sin \alpha \sin \gamma \\ \cos \beta \sin \gamma & \sin \alpha \sin \beta \sin \gamma + \cos \alpha \cos \gamma & \cos \alpha \sin \beta \sin \gamma - \sin \alpha \cos \gamma \\ -\sin \beta & \sin \alpha \cos \beta & \cos \alpha \cos \beta \end{bmatrix} \quad (5)$$

All the coordinate calculations will be completed in unity, and the relational variables will be determined by the initialization measurement. In the process, as long as coordinate position and the displacement vector are imported, we will calculate the world coordinate system corresponding to the points of other coordinates.

3.2. Generation and Processing of Screen Images

The camera model is an ideal perspective projection transformation, transforming the point of the global coordinate system into the point of the image plane coordinate system [38-40]. The transformation formula $P_w = (X_w, Y_w, Z_w)^T$ to image coordinate system

$C_0 = (u, v)^T$ in the global coordinate system is:

$$C_0 = PP_w \quad (6)$$

where M_1 is perspective projection matrix, which can be expressed by internal and external parameter matrices.

$$P = M_1 [R | T] \quad (7)$$

Internal parameters refer to the basic parameters of camera imaging and describe the corresponding relationship between camera points in the coordinate system and pixel points in the image. M_1 Including the center point (ideally the center of the image), the actual focal length, lens distortion (mainly including radial distortion and tangential distortion) and other systematic error parameters, the camera internal parameters can be obtained by camera calibration.

The form of the internal parameter matrix is as follows:

$$M_1 = \begin{bmatrix} f_x & R & u_0 \\ 0 & f_y & v_0 \\ 0 & 0 & 1 \end{bmatrix} \quad (8)$$

where, f_x and f_y are focal lengths in the x and y directions, respectively. R is the distortion factor. u_0 and v_0 are the center coordinates of the graph.

R_{xy} is the rotation change matrix mentioned in the last video, and T is the translation matrix.

$$[R_{xy} | T] = \begin{bmatrix} \cos \beta \cos \gamma & \sin \alpha \sin \beta \cos \gamma - \cos \alpha \sin \gamma & \cos \alpha \sin \beta \cos \gamma + \sin \alpha \sin \gamma | t_x \\ \cos \beta \sin \gamma & \sin \alpha \sin \beta \sin \gamma + \cos \alpha \cos \gamma & \cos \alpha \sin \beta \sin \gamma - \sin \alpha \cos \gamma | t_y \\ -\sin \beta & \sin \alpha \cos \beta & \cos \alpha \cos \beta & | t_z \end{bmatrix}$$

(9)

The relationship between a point in 3d space and its projected pixel points on the image space can be described in detail as follows:

$$\begin{bmatrix} x_i \\ y_i \\ 1 \end{bmatrix} = \begin{bmatrix} f_x & r & u_0 \\ 0 & f_y & v_0 \\ 0 & 0 & 1 \end{bmatrix} \begin{bmatrix} \cos \beta \cos \gamma & \sin \alpha \sin \beta \cos \gamma - \cos \alpha \sin \gamma & \cos \alpha \sin \beta \cos \gamma + \sin \alpha \sin \gamma |t_x \\ \cos \beta \sin \gamma & \sin \alpha \sin \beta \sin \gamma + \cos \alpha \cos \gamma & \cos \alpha \sin \beta \sin \gamma - \sin \alpha \cos \gamma |t_y \\ -\sin \beta & \sin \alpha \cos \beta & \cos \alpha \cos \beta |t_z \end{bmatrix} \begin{bmatrix} X_i \\ Y_i \\ Z_i \\ 1 \end{bmatrix}$$

(10)

The internal parameter matrix of the camera is the inherent parameter of the camera which can be obtained by calibrating. Although the transformation matrix has 12 unknowns, it has only 11 degrees of freedom. Only 6 pairs of points in 3d space and their corresponding 2d image points are needed to solve the 12 parameters. These parameters include the camera's position and attitude. According to matrix multiplication, the following forms can be obtained:

$$\begin{bmatrix} x_i \\ y_i \\ 1 \end{bmatrix} = \begin{bmatrix} \cos \beta \cos \gamma X_i + \sin \alpha \sin \beta \cos \gamma Y_i - \cos \alpha \sin \gamma Y_i + \cos \alpha \sin \beta \cos \gamma Z_i + \sin \alpha \sin \gamma Z_i + t_x \\ \cos \beta \sin \gamma X_i + \sin \alpha \sin \beta \sin \gamma Y_i + \cos \alpha \cos \gamma Y_i + \cos \alpha \sin \beta \sin \gamma Z_i - \sin \alpha \cos \gamma Z_i + t_y \\ -\sin \beta X_i + \sin \alpha \cos \beta Y_i + \cos \alpha \cos \beta Z_i + t_z \end{bmatrix}$$

(11)

The coordinate value of the target on the image is:

$$x_i = \frac{\cos \beta \cos \gamma X_i + \sin \alpha \sin \beta \cos \gamma Y_i - \cos \alpha \sin \gamma Y_i + \cos \alpha \sin \beta \cos \gamma Z_i + \sin \alpha \sin \gamma Z_i + t_x}{-\sin \beta X_i + \sin \alpha \cos \beta Y_i + \cos \alpha \cos \beta Z_i + t_z}$$

$$y_i = \frac{\cos \beta \sin \gamma X_i + \sin \alpha \sin \beta \sin \gamma Y_i + \cos \alpha \cos \gamma Y_i + \cos \alpha \sin \beta \sin \gamma Z_i - \sin \alpha \cos \gamma Z_i + t_y}{-\sin \beta X_i + \sin \alpha \cos \beta Y_i + \cos \alpha \cos \beta Z_i + t_z}$$

(12)

Homogeneous linear equations can be solved by removing the denominator, and two such equations can be obtained for each pair of points. Finding the position of N different points in the world coordinate system and determining their coordinates in the camera image Homogeneous linear equations can be solved by removing the denominator, and two such equations can be obtained for each pair of points. When $N \geq 6$, the position and attitude of the augmented reality virtual image embedded in the whole system can be solved.

4. Design and Composition of the System

4.1 Design of Mechanical Structure

Figure 3 shows an orbiting mobile camera designed by the experimental team at Harbin engineering university. Mobile camera adopts the method of bilateral orbit and upper and lower clamping balance, camera movement is rolling on the sprocket in the chain, sprocket drive is done by stepping motor, encoder read the rotation of the sprocket wheel and then calculate the movement of the camera position, on a host computer through wireless signal to control the operation of the whole system. The trolley mechanical system consists of five parts: frame and chain mechanism, sliding-contact line power supply mechanism, sprocket drive mechanism and encoder feedback mechanism.



Figure 3. The structure of the mobile camera system

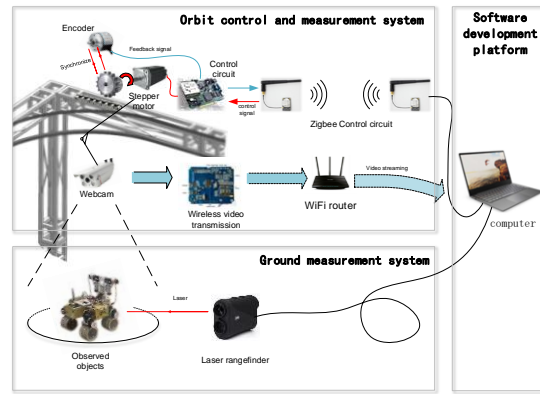


Figure 4. The control system architecture.

4.2 Control System Design

The control system has three functions : (a) according to the input signal of the computer to control the position, speed, switch signal and other information of the motion camera; (b) receive and display the video signal returned by the camera; (c) receive and calculate the data of the rangefinder. As shown in figure 4.

The main component of the controller is STM32 single-chip microcomputer. On the one hand, it receives the control signal from the computer and sends out the pulse signal to drive the stepper motor. The other receives feedback from the encoder and sends it to the computer for processing. To realize barrier-free operation in the air, it communicates with the computer through Zigbee wireless transmission and uses sliding contact line for sliding power supply.

3.3 Software Generation of The System

Unity3D software is used as the development platform of augmented reality in this paper. On the one hand, Unity3D can obtain the video stream by executing the c# script and display the images that can reflect the real world on the screen. On the other hand, the camera composition information from the sensor is also received by the executing code, and the attitude of the virtual object in the display screen is expressed through the corresponding algorithm (as described in section 4). Therefore, virtual objects are presented on the screen for augmented reality.

The design flow of the software is determined based on the workflow of the entire system. As shown in figure 5.

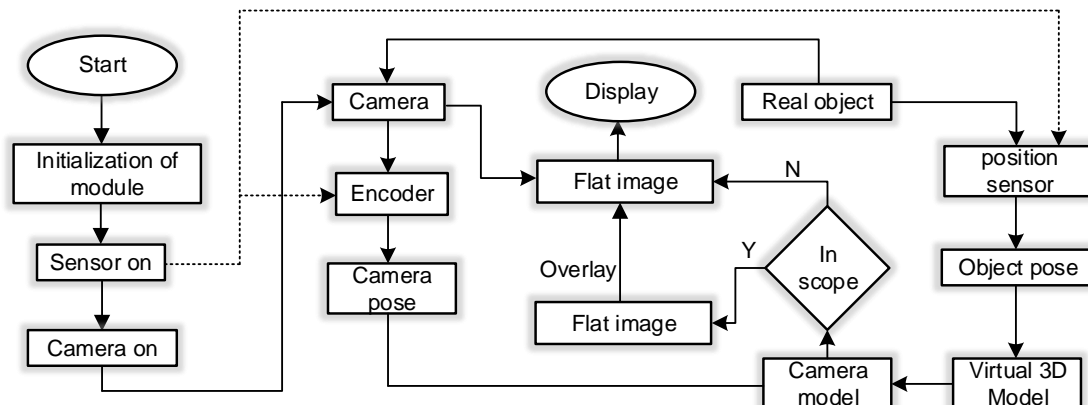


Figure 5. Flowchart of our proposed method.

5. Error Analysis and Experiment

In this experiment, the camera track is a runway, 4 meters high from the ground, 6 meters long and 3 meters wide, with four turning radii of 1 meter. Z880A industrial camera and sy-03 manual turntable are used. The camera uses a fixed focal length with the resolution and frame rate set to 640*480:30 frames. Bes38-0656n-1000 encoder is adopted. The experimental equipment is shown in figure 6.

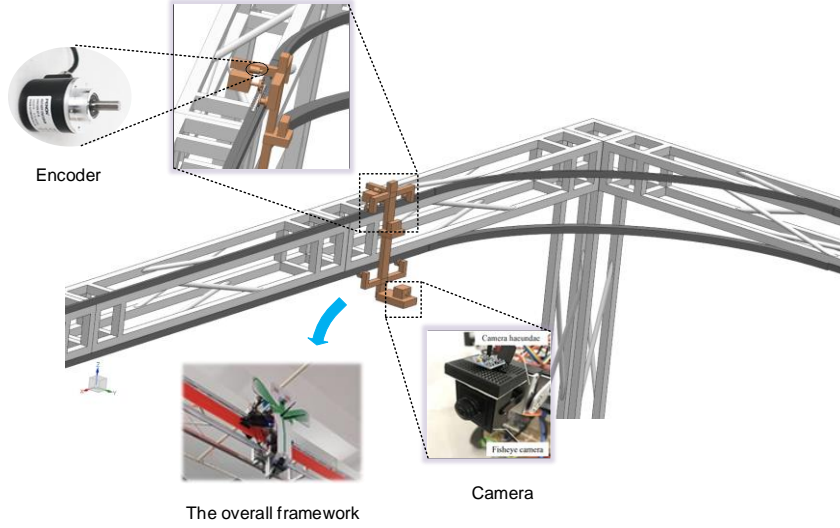


Figure 6. Equipment structure diagram.

5.1. Analysis of The Error of the Equipment System

To independently calculate the influence of system structure error on augmented reality observation, coordinate measurement error and calibration error are not considered in this experimental analysis. Therefore, the coordinate transformation relation is as follows:

$$\begin{bmatrix} X_{w0} \\ Y_{w0} \\ Z_{w0} \\ 1 \end{bmatrix} = \begin{bmatrix} \cos \beta & \sin \alpha \sin \beta & \cos \alpha \sin \beta & t_x \\ 0 & \cos \alpha & -\sin \alpha & t_y \\ -\sin \beta & \sin \alpha \cos \beta & \cos \alpha \cos \beta & t_z \\ 0 & 0 & 0 & 1 \end{bmatrix} M_{cr} \begin{bmatrix} X_{c0} \\ Y_{c0} \\ Z_{c0} \\ 1 \end{bmatrix} \quad (13)$$

Assuming $M_{cr} = 1$,

$$\begin{aligned} X_{w0} &= \cos \beta X_{c0} + \sin \alpha \sin \beta Y_{c0} + \cos \alpha \sin \beta Z_{c0} + t_x \\ Y_{w0} &= \cos \alpha Y_{c0} - \sin \alpha Z_{c0} + t_y \\ Z_{w0} &= -\sin \beta X_{c0} + \sin \alpha \cos \beta Y_{c0} + \cos \alpha \cos \beta Z_{c0} + t_z \end{aligned} \quad (14)$$

The error transfer coefficient is

$$\left\{ \begin{array}{l} \frac{\partial X_{w0}}{\partial \alpha} = \cos \alpha \sin \beta Y_{c0} - \sin \alpha \sin \beta Z_{c0}, \\ \frac{\partial X_{w0}}{\partial \beta} = \sin \beta X_{c0} - \sin \alpha \cos \beta Y_{c0} - \cos \alpha \cos \beta Z_{c0} \\ \frac{\partial Y_{w0}}{\partial \alpha} = \sin \alpha Y_{c0} + \cos \alpha Z_{c0}, \frac{\partial Y_{w0}}{\partial \beta} = 0, \frac{\partial Z_{w0}}{\partial t_z} = 1 \\ \frac{\partial Y_{w0}}{\partial t_y} = 1, \frac{\partial Z_{w0}}{\partial \alpha} = -\cos \alpha \cos \beta Y_{c0} - \sin \alpha \cos \beta Z_{c0} \\ \frac{\partial Z_{w0}}{\partial \beta} = -\cos \beta X_{c0} + \sin \alpha \sin \beta Y_{c0} + \cos \alpha \sin \beta Z_{c0} \end{array} \right. \quad (15)$$

Assuming that the standard deviation of the turntable Angle and the orbital translation output are independent of each other, the standard deviation of the coordinate measurement can be obtained according to the error transfer relation.

$$\begin{aligned} \sigma_{X_{w0}} &= \sqrt{(\cos \alpha \sin \beta Y_{c0} - \sin \alpha \sin \beta Z_{c0})^2 \sigma_{\alpha}^2 + (\sin \beta X_{c0} - \sin \alpha \cos \beta Y_{c0} - \cos \alpha \cos \beta Z_{c0})^2 \sigma_{\beta}^2 + \sigma_{t_x}^2} \\ \sigma_{Y_{w0}} &= \sqrt{(\sin \alpha Y_{c0} + \cos \alpha Z_{c0})^2 \sigma_{\alpha}^2 + \sigma_{t_y}^2} \\ \sigma_{z_{w0}} &= \sqrt{(\cos \alpha \cos \beta Y_{c0} + \sin \alpha \cos \beta Z_{c0})^2 \sigma_{\alpha}^2 + (-\cos \beta X_{c0} + \sin \alpha \sin \beta Y_{c0} + \cos \alpha \sin \beta Z_{c0})^2 \sigma_{\beta}^2 + \sigma_{t_z}^2} \end{aligned} \quad (16)$$

Analyzing the influence of the output error of the turntable's Angle on the observation when the orbit moves and the turntable rotates to different angles:

From the above analysis, it can be seen that the system error is related to the accuracy of the orbit and the output error of the turntable angle, as well as the rotation Angle of the camera turntable and the observation distance.

In this experiment, the observation and distance measurement $Z=3000\text{mm}$, the Z direction of the orbit is parallel to the ground adjustment, the maximum Angle of the experiment is 45° , the values of X and Y are 100mm , and the error transfer coefficient is set as:

$$\sigma_{X_{w0}} = 1.51 \quad \sigma_{Y_{w0}} = 1.55 \quad \sigma_{z_{w0}} = 1.13$$

5.2 Static Workpiece Experiment

The experiment completed the test by making 30 repeated observations of the flexible arm system. Three observation points were selected on the orbit of 0mm , 300mm , 1500mm , and repeatability tests were conducted on each point.

Before the experiment, the calibration module in Unity3D software was used to calibrate the camera and cradle head, and the internal parameters of the camera were calibrated. The results are shown in Table 1.

Table 1. The camera parameters

Camera Model	f_x	f_y	r	Pixel		Distortion Coefficient	
				u_0	v_0	K_1	K_2
Z880A	3676.462	3676.478	0.263	645.342	508.259	1.30	1.88

The camera turntable is a 6-degree-of-freedom manual turntable, and the positioning accuracy is repeated to the indexing level, but only two of them are used in this experiment. After the camera is installed on the turntable, the posture of the turntable is calibrated, and the result is.

$$M_{cr} = \begin{bmatrix} 0.9907 & 0.1353 & -0.0064 & 50.843 \\ -0.1396 & 0.9915 & 0.0093 & 47.094 \\ 0.0083 & -0.0085 & 0.9990 & 76.177 \\ 0 & 0 & 0 & 1 \end{bmatrix} \quad (17)$$

As shown in figure 7 below, the virtual image and the solid image are displayed in a fixed parallel direction, with only a distance between them in the X-axis direction. The moving speed of the motion camera is 0.1m /s, and the moving track plane is perpendicular to the z-axis. The workpiece coordinate system is obtained by measuring the feature points on the workpiece with the rangefinder.

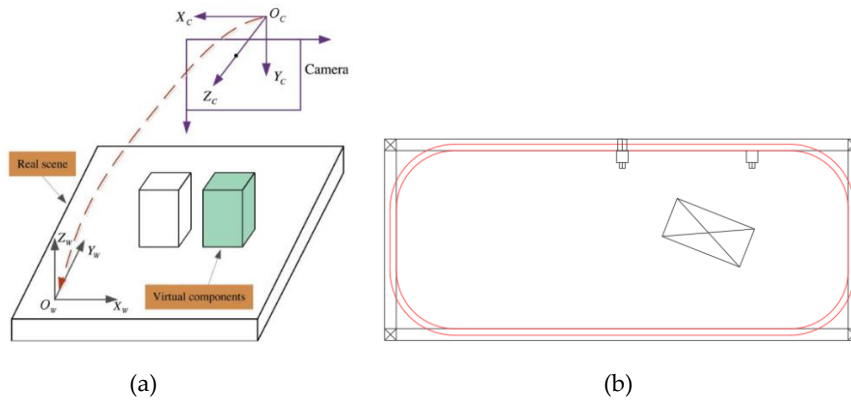


Figure 7. Schematic diagram of the first experiment. (a) Diagram for AR registration (b) Diagram camera movement

The initial state (zero point) of the workpiece is the coincidence between the virtual image and the physical image. The first observation points: the virtual image to the moving direction of 300 mm x-axis, using video image measuring tool software and entity scale, measure the virtual image geometric center, center of plane geometry and the real image and actual distance on the x-axis. The second observation point : move the camera to the moving direction of 2000 mm x-axis, virtual like Settings, still, distance measuring geometric center. Initial state, first observation point, and second observation point. As shown in figure 8:

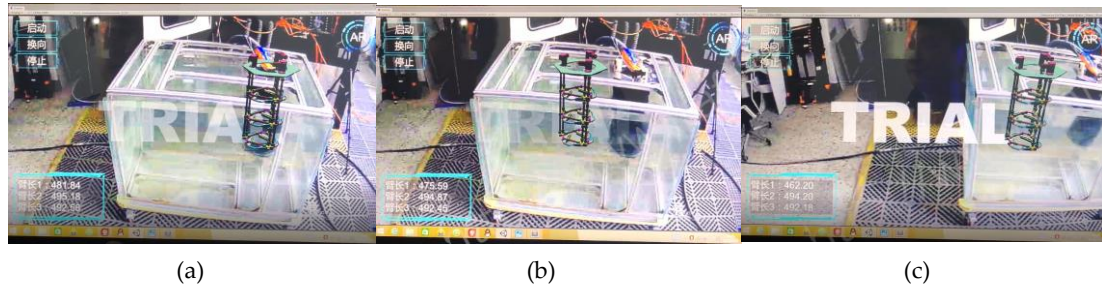


Figure 8. Screen display during the experiment. (a) Initialization display (b) First screenshot (c) Second screenshot

Table 2. Measuring result.

The camera position	Camera range	Measurement of the mean	The standard deviation
Initialize the point	0 mm	0.5	1.2
The first point	300 mm	288.9	1.35
The second point	2000 mm	1499.5	1.41

It can be seen from the table that the moving distance of the moving camera has a certain influence on the observation, but because the fixed turntable is used in this experiment and the Angle is small, the error generated by the moving distance has a small influence. The observation accuracy can be significantly improved by increasing the orbit accuracy, minimizing the dynamic change of the turntable and decreasing the rotation Angle.:

5.3 Moving workpiece experiment

Using the same observation equipment as in the first experiment, the mobile camera was used to track the robot. The robot moves in a uniform straight line along the X-axis, and the moving camera tracks at the same speed. Keep the distance between the virtual image and the solid image constant, as shown in figure 9.



Figure 9. Experimental process display. (a) Start measuring screenshots (b) End measurement screenshot

The video image measurement tool software and solid ruler are still used to measure the change in the distance between the geometric center point of the virtual image and the solid image. The data result is shown in figure 10.

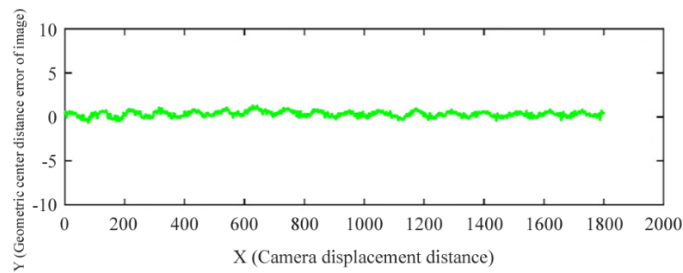


Figure 10. Error of real-time distance.

For comparison with a marked visual system, the standard deviation R is referenced.

$$R = \sqrt{\frac{1}{N} \sum_{i=1}^N (P_N - P_E)^2} \quad (18)$$

where, N is the number of samples under the total trajectory length, and the measured true error value is P_N , the theoretical error value $P_E=0$ in this experiment. The actual walking length of the robot is more than 1500mm, so the first 1500mm will be taken as the data sample. Collect 30 points and calculate $R = 0.5\%$, which is more accurate than visual tracking.

6. Conclusions

In this paper, an unlabeled large field of view augmented reality observation method is proposed, which effectively solves the problem of light sensitivity of labeled augmented reality. As a new method, it is especially suitable for the industrial plant with strong anti-interference ability. Finally, two experiments are carried out, and the results show that the system can well enhance the display of reality images in large space, make the images always in the right position and size, and has good adaptability.

However, this paper focuses on the calculation principle of augmented reality and spatial conversion brought by the encoder, as well as error analysis. The virtual image generated by the experiment is fixed relative to the entity, and will not change with time, camera movement and other factors. In the future, dynamic algorithms will be used to improve the performance of augmented reality displays.

References

1. Levi Manring, John Pederson, Dillon Potts, Beth Boardman, David Mascarenas, Troy Harden and Alessandro Cattaneo; Augmented Reality for Interactive Robot Control; Modern Information Technology. Special switchable viewer in Structural Dynamics and Experimental Techniques, Volume 5, Conference Proceedings of the Society for Experimental Mechanics Series, https://doi.org/10.1007/978-3-030-12243-0_2
2. LIN Ruizong; PENG Chuanxiang; GAO Xian; LI Zhenglin.; Research on the Completion Acceptance of Substation Engineering -based on AR Space Measurement Technology; Modern Information Technology 2096-4706 (2018) 12-0190-03 Author 1, A.; Author 2, B. *Book Title*, 3rd ed.; Publisher: Publisher Location, Country, 2008; pp. 154–196.
3. Mar 1 a - Blanca Ibanez, Angela Di - Serio; Diego Villaran - Molina; Carlos Delgado - Kloos; Support for Augmented Reality Simulation Systems: The Effects of Scaffolding on Learning Outcomes and Behavior Patterns; IEEE TRANSACTIONS ON LEARNING TECHNOLOGIES, vol.9, NO. 1, january-march 2016.
4. Yang Wang; Yuji Sato; Mai Otsuki; Hideaki Kuzuoka, Yusuke Suzuki; Effect of Body Representation Level of an Avatar on Quality of ar-based Remote Instruction; Multimodal Technol. Interact. 2020, 4, 3; Doi: 10.3390 / mti4010003
5. Industry 4.0 ongoing: how augmented reality is transforming manufacturing. <http://www.cnki.net>
6. CHEN Junhua; CHEN, Changyu; SUN Gang; WAN Bile. Research on the Application Technology of Augmented Reality in Spacecraft Cable Assembly; Science and Technology & Innovation 2095-6835(2019)08-0040-05
7. LUO Kang; LI Xin; Implementation of 3D Display of Products Based on Augmented Reality Technology; JOURNAL OF JINLING INSTITUTE OF TECHNOLOGY 1672-755x (2019)01-0006-05
8. Changmin Lim; Chanran Kim; jong-l Park; Hanhoon Park; Mobile Augmented Reality Based on Invisible Marker; IEEE International Symposium on Mixed and Augmented Reality Adjunct Proceedings. 978-1-5,090-3740-7/16
9. Robert Woll; Thomas Damerau; Kevin Wrasse,; Rainer Stark; Augmented Reality in a Serious Game for Manual Assembly Processes; IEEE International Symposium on Mixed and Augmented Reality 2011 Science and Technology Proceedings 26-29 October, Basel, Switzerland. 978-1-4673-0059-9/10
10. John Sausman; Alexei Samoylov; Susan Harkness Regli; Meredith Hopps; Effect of Eye and Body Movement on Augmented Reality in the Manufacturing Domain; IEEE International Symposium on Mixed and Augmented Reality 2012 Science and Technology Proceedings 5-8 November 2012, Atlanta, Georgia 978-1-4673-4662-7/12
11. DIMITRIS CHATZOPOULOS; CARLOS BERMEJO; ZHANPENG HUANG; PAN HUI; Mobile Augmented Reality Survey: From Where We Are to Where We Go; IEEE Access Digital Object Identifier/Access. 10.1109 2017.2698164

12. Shao Jiang; Yan ketong; Yao Jun; Niu yafeng; Experimental study on visual search for aiming symbols in head-mounted AR system interface; JOURNAL OF SOUTHEAST UNIVERSITY (Natural Science Edition) 1001-0505(2020)01-0020-06
13. Ivo Maly; David Sedla 'cek; Paulo Leitao; Augmented Reality Experiments with Industrial Robot in Industry 4.0 Environment; The 978-1-5-090-2870 \$31.00/2/16 © 2016 IEEE
14. Holger Regenbrecht; Industrial Augmented Realities Applications; University of Otago, New Zealand Chapter XIV
15. PAULA FRAGA-LAMAS; MIGUEL A. VILAR-MONTESINOS; A Practical Evaluation of Commercial Industrial Augmented Reality Systems in an Industry 4.0 Shipyard; SPECIAL SECTION ON HUMAN-CENTERED SMART SYSTEMS AND TECHNOLOGIES
16. V. Havard; D. Baudry; A. Louis, and B. Mazari; Augmented reality maintenance demonstrator and associated modelling, in Proc. IEEE Virtual Reality (VR), Mar. 2015, pp. 329–330.
17. Virtual Reality Technology Transforms Design of UK Warships. Accessed: Dec. 1, 2017. [Online]. Available: <http://www.baesystems.com/en/article/virtual-reality-technology-transforms-design-of-uk-warships>
18. LIU Rui; YIN Xu ;FAN Xiu;WANG Lei.HE Qi chang; AR Guidance Based visual inspection method for cable laying quality consistency check; Computer Integrated Manufacturing Systems
19. Zhenliang Zhang; Dongdong Weng; Haiyan Jiang; Yue Liu; Yongtian Wang; Inverse Augmented Reality: A Virtual Agent's Perspective; IEEE International Symposium on Mixed and Augmented Reality Adjunct 2018 (ismar-adjunct) 987-1-5386-7592-2/18
20. Alex Hill; Harrison Leach; Interactive Panned and Zoomed Augmented Reality Interactions Using COTS Heads Up Displays; IEEE International Symposium on Mixed an Augmented Reality 2014 Science and Technology Proceedings 10-12 September 2014,Munich.Germany.978-1-4799-6184-9/13
21. Doree Duncan Seligmann; Steve Feiner; Automated generation of intent - -based 3 d Illustrations, ACM SIGGRAPH Computer Graphics, v. 25 n. 4, p. 123-132, out of 1991
22. Dirk Groten; Ronald Van Der Lingen; Layar On Google Glass: It 's Not Augmented Reality, Web Blog Posting, June 25, 2013, <https://www.layar.com/news/blog/2013/06/25/layar-on-google-glass>
23. Smart Glasses Moverio BT - 200, Epson, <http://www.epson.com/cgi-bin/Store/jsp/Landing/moverio-bt-200-smart-glasses.do>
24. Christopher Freeman; Rab Scott; An exercise in cost and waste reduction using Augmented Reality in Composite Layup manufacturing; March 23-27, 2015 IEEE Virtual Reality Conference, Arles, France 978-1-4799-1727-3/15
25. Husam A.A das; Sachin Shetty.S.K eith Hargrove; Virtual and Augmented Reality Based Assembly Design System for Personalized Learning. Science and Information Conference on October 7-9, 2013
26. Ma Jindun; Zhang Lei; Guo Libin; Zhang Jie; Research Summary of Augmented Reality Equipment Maintenance Guidance System; Journal of Ordnance Equipment Engineering; ISSN 2096-2034, 50-1213 / CN TJ
27. Yaxuan Zhou; Paul Yoo; Yingru Feng; Aditya Sankar, Alireza Sadr, Eric j. Seibel; Towards ar-assisted visualisation and guidance for imaging of dental decay; Healthcare Technology Letters, 2019, vol.6, Iss. 6, pp. 243 -- 248 doi: 10.1049/ htr.2019.0082
28. Mohammed A, Schmidt B, Wang l. Active collision avoidance for human-robot collaboration driven by vision sensors[J]. International Journal of Computer Integrated Manufacturing, 2017, 30(9):970-980.
29. Wei Fang; Lianyu Zheng; Xiangyong Wu; Multi-sensor based real-time 6-dof pose tracking for wearable wearable reality; Computers in Industry. 92-93 (2017) 91-103
30. Wang. A comprehensive survey of augmented reality assembly research [J]. Advances in Manufacturing, 2016:1-22.
31. LI Jin; LIU Xuan; ZHANG Jianhua; ZHANG Jie; CHEN Hao; ZHANG Yaonan; Research on Indirect Solution of Inverse Kinematics Based on RBF Neural Network; The MACHINE TOOL & HYDRAULICS; ISSN1001-3881.20199.23.007
32. G. Klein, d. Murray; Parallel tracking and mapping for small AR workspaces,Proc. Of IEEE/ACM International Symposium on Mixed and Augmented Reality(2007) 1-10.

33. F. Endres, j. Hess, n. Engelhard, j. Sturm, d. Cremers, w. Burgard, An evaluation of the rgg-d SLAM system, Proc of IEEE International Conference on Robotics and Automation (2012) 1691 -- 1696.
34. Analysis and research on spatial coordinate transformation technology (I) (ii). Theory and practice, 1999,19 (4) : 10-13.
35. N. Navab, C. Hennemersperger, B. Frisch, B. Furst, Personalized, relevance-based multimodal robotic imaging and augmented reality for computer assisted interventions, Med. Image Anal. 33 (2016) 64–71.
36. D.B. Espíndola, L. Fumagalli, M. Garetti, C.E. Pereira, S.S.C. Botelho, R.V.Henriques, A model-based approach for data integration to improve maintenance management by mixed reality, Comput. Ind. 64 (4) (2013) 376–391.
37. P. Han, G. Zhao, CAD-based 3D objects recognition in monocular images for mobile augmented reality, Comput. Graphics 50 (2015) 36–46.
38. S. Leutenegger, S. Lynen, M. Bosse, R. Siegwart, P. Furgale, Keyframe-based visual-inertial odometry using nonlinear optimization, Int. J. Robot. Res. 34 (3)(2015) 314–334
39. C. Forster, L. Carlone, F. Dellaert, D. Scaramuzza, IMU preintegration on manifold for efficient visual-inertial maximum-a-posteriori estimation, Proc.of Robotics: Science and Systems Conference (2015).
40. Richard Hartley and Andrew Zisserman, Multiple view geometry in. Computer vision, vol.2, Cambridge Univ Press, 2000.